Eur Biophys J (2015) 44:37–47
DOI 10.1007/s00249-014-0999-0

ORIGINAL PAPER

EBSA
Biophysics in Europe

Free energy simulations of amylin I26P mutation in a lipid bilayer

Seifollah Jalili · Afsaneh Maleki · Mojdeh Akhavan · Bijan Najafi · Jeremy Schofield

Received: 11 May 2014 / Revised: 6 November 2014 / Accepted: 10 November 2014 / Published online: 27 November 2014

Abstract The amylin peptide in a dioleoylphosphatidylcholine (DOPC) bilayer is studied using united atom molecular dynamics (MD) simulations. Dynamics and transport properties of the peptide and the phospholipid bilayer are investigated. The lateral diffusion of DOPC is in the order of 10^{-8} cm^2 s^{-1}, which is in agreement with the experimental results. The order parameter and density profile for phospholipid molecules in the bilayer are calculated. The secondary structure of amylin peptide shows that the amino acids in two terminals are structureless and two α-helical segments in the peptide are connected through an unstructured link. This structure is similar to the experimental structure in the membrane-mimicking media. Free energy calculations of the Ile26 → Pro mutation in the amylin peptide are performed in the bilayer and in aqueous solution using molecular dynamics simulations and a thermodynamic cycle. It is shown that in the mutated peptide in aqueous solution, the α-helix structure changes to a 5-helix, whereas this configuration is preserved in the bilayer environment. It is interesting that the accessible surface area increases for hydrophobic residues in the bilayer and for hydrophilic residues in aqueous solution as the coupling parameter changes from 0 to 1. These results are significant to understanding the aggregation mechanism of human amylin monomers in membranes to the dimers, trimers, oligomers, and fibrils associated with the type 2 diabetes at the atomic level.

Keywords Amylin · Dioleoylphosphatidylcholine lipid · Free energy calculation · Molecular dynamics simulation · Thermodynamic integration · I26P mutation

Electronic supplementary material The online version of this article (doi:10.1007/s00249-014-0999-0) contains supplementary material, which is available to authorized users.

S. Jalili
Department of Chemistry, K.N. Toosi University of Technology, P.O. Box 15875-4416, Tehran, Iran

S. Jalili · M. Akhavan
Department of Nano-Science, Computational Physical Sciences Research Laboratory, Institute for Studies in Theoretical Physics and Mathematics (IPM), P.O. Box: 19395-5531, Tehran, Iran

A. Maleki (✉)
Department of Chemistry, Islamic Azad University, Omidiyeh Branch, Omidiyeh, Khuzestan, Iran
e-mail: maleki.afsaneh@iauo.ac.ir

B. Najafi
Department of Chemistry, Isfahan University of Technology, Isfahan, Iran

J. Schofield
Department of Chemistry, Chemical Physics Theory Group, University of Toronto, 80 Saint George Street, Toronto, ON M5S 3H6, Canada

Introduction

Amylin fibrillar deposits are found in the pancreas of patients afflicted with type 2 diabetes (T2DM) (Patil et al. 2009; Westermark et al. 1987; Betsholtz et al. 1989). The main component of these deposits is identified as a 37-residue peptide called islet amyloid polypeptide (IAPP) or amylin (Westermark et al. 1987). Monomeric human IAPP (hIAPP) is suggested to be a hormone with roles in gastric emptying and regulation of glucose homeostasis (Karlsson 1999). hIAPP is produced and secreted, together with insulin, by the β-cells in the pancreatic islets of Langerhans. The amino acid sequence of IAPP varies slightly from

organism to organism (Betsholtz et al. 1989). For instance, six residues are different between hIAPP and mouse IAPP (mIAPP).

A number of computational studies have explored the monomeric and oligomeric/fibrillar structures of full-length hIAPP (Dupuis et al. 2011; Laghaei et al. 2011) and its fragments (Mo et al. 2009; Xu et al. 2009) in aqueous solution. Detailed ultrastructural investigations have shown that islet amyloid is often in contact with β-cell membranes (Westermark 1973). There is evidence to suggest that freshly dissolved hIAPP has a pronounced ability to insert into lipid monolayers, whereas fibrillar hIAPP does not insert (Engel et al. 2006). Membranes are thought to facilitate the aggregation of amylin, and membrane-bound oligomers are possibly responsible for the islet β-cell toxicity that develops during type 2 diabetes (Khemtemourian et al. 2008). Membrane-bound hIAPP dimers show a more pronounced ability to perturb membranes than monomers (Zhang et al. 2012).

Recently, the adsorption orientation and conformation of hIAPP monomer at an anionic POPG lipid have been studied (Jia et al. 2013). These studies have shown that hIAPP monomer binds to lipid from the *N*-terminal residues by strong electrostatic interactions of the positively charged residues Lys1 and Arg11 with negatively charged lipid headgroups. hIAPP binds parallel to the lipid bilayer surface as a stable helix through residues 7–22, consistent with previous experimental studies (Zhang et al. 2012; Jia et al. 2013).

The full-length IAPP peptide can be divided into three regions: an N-terminal region from residues 1 to 19 that largely determines the membrane binding (Jia et al. 2013; Lopes et al. 2007), a primary amyloidogenic region from residues 20 to 29, and a C-terminal region from residues 30 to 37 that increases amyloid formation (Jia et al. 2013; Jaikaran et al. 2001). However, the mechanism of hIAPP-membrane interaction is largely unknown. There are a few studies performed in the presence of a few of lipid molecules or bilayers for hIAPP fragments (Jiang et al. 2009; Sciacca et al. 2010). In this work, we have investigated the interaction of a full-length hIAPP monomer with a dioleoylphosphatidylcholine (DOPC) bilayer that is the most abundant zwitterionic phospholipid species in the membrane of pancreatic islet cells. For a better understanding of the structural basis for the interactions between the amylin and membrane, we have performed MD simulations from an initial configuration in which the peptide monomer is embedded deeply and fully in the bilayer, parallel to the membrane axis. This location is more favorable for investigating membrane destruction. This study is novel in the sense that it provides a model for amylin integrally associated with the bilayer. This study could have substantial implications for the exiting mechanism of amylin and its propensity to do so, the mechanism of membrane damage, and developing new drugs and/or finding new targets for the treatment of DM2.

Molecular biology studies on hIAPP have shown that the Ser20 → Gly (S20G) mutant may promote the formation of the aggregates associated with the early stages of type 2 diabetes (Sakagashira et al. 2000; Dupuis et al. 2011). The frequency of the S20G mutation in the amylin gene is 1.92 % in unrelated patients with type 2 diabetes in Korea, although it is not associated with an increased risk of type 2 diabetes (Garcia-Gonzalez et al. 2007). Molecular dynamics studies indicate that S20G drives the residues 15–17 and 20–29 of hIAPP to transform from a helical structure to β-strands or coil structures with higher extension and flexibility, which may promote the aggregation of hIAPP, as experiments have reported (Wang et al. 2012). Also, the replacement of Leu16 by Gln (L16Q) stabilizes the helix structure in residues 15–17 and 20–23 of the hIAPP monomer. L16Q showed that the region of residues 15–17 is closely related to the aggregation of hIAPP (Wang et al. 2012). MD simulations of the monomeric structure of hIAPP(1–25) and the effect of S20G mutation on the helical structure in a DOPC/DOPS bilayer have shown that a helical disruption at His18 is common to both human variants (Duan et al. 2012).

Proline substitutions in the region of residues 20–29 in rats and some other species are thought to be the major factors preventing the refolding of the molecule into a β-conformation and its assembly into typical amyloid fibrils (Jaikaran and Clark 2001). A study has shown that a single amino acid substitution in hIAPP, where Ile on position 26 is replaced by Pro (I26P), yields a potent fibrillization inhibitor. hIAPP and its I26P mutant have been synthesized and the fibrillization rate of each peptide has been determined using standard fluorescence-detected thioflavin-T-binding studies (Abedini et al. 2007).

Understanding the structural nature of the hIAPP monomer in a neutral bilayer is the premise of disclosing the aggregation mechanism of hIAPP. Our innovation is to obtain the effect of a single proline mutant at position 26 in an amylin polypeptide on its binding to a bilayer using free energy simulations. The ability to rapidly and accurately calculate a difference in binding free energies between two drug candidates and their target (usually a protein) and the binding of proteins to bilayers is of interest in structural biology and of importance to the pharmaceutical industries (Fowler et al. 2004).

Methods

Molecular dynamics simulations

The initial configuration of peptide was taken as the minimum-energy structure from an ensemble of 30 structures determined by NMR, with the protein data bank (PDB) code

of 2KB8. The ionic states NH_3^+ and COO^- were used for the N- and C- terminal arms of the amylin peptide, respectively. The starting configuration of the lipid bilayer (lipids + water molecules) was obtained from a pre-equilibrated DOPC membrane model of 128 lipids (http://www.bioinf.uni-sb.de/RB/dopc/berger/berger-NPT-100ns.pdb). In order to embed the peptide in the bilayer, we used the INFLATEGRO program from Tieleman's group (Kandt et al. 2007). In this method, two lipids were deleted from the bottom leaflet of the bilayer, leaving 126 DOPC molecules packed around the amylin peptide in such a way that their average area per lipid was close to that of the experimental data (Petrache et al. 2004; Tristram-Nagle et al. 1998). The bilayer was parallel to the *xy* plane so that the *z* axis was along the bilayer normal. The system was solvated with SPC (simple point charge) waters (Berendsen et al. 1981) and neutralizing, and additional sodium and chloride ions (corresponding to ~0.1 M NaCl) were added. The system, containing about 17,710 atoms, was energy-minimized before MD, using 50,000 steps of the steepest descent method to relax any steric conflicts generated during the setup. After that, in the equilibration phase, 1 ns NVT simulation at 323 K was performed, followed by NPT simulation for 1 ns at 323 K and 1 bar. All bond lengths were constrained to their equilibrium values using the LINCS algorithm (Hess et al. 1997). Position restraints were applied to the peptide during the equilibration phase. After equilibration, restraints were removed from the peptide and the production phase began. Production simulations were allowed to proceed for 40 ns in the NPT ensemble.

Parameters from the Gromos 53a6 parameter set (Oostenbrink et al. 2004) were applied to the peptides and ions in the system. Lipids were described by parameters derived by Berger et al. (1997). The temperatures of the peptide, DOPC, and solvent (including water molecules and ions) were separately maintained at 323 K using a coupling constant of 0.1 ps. The pressure was regulated semi-isotropically at 1 bar using a coupling constant of 5.0 ps. Electrostatic interactions were calculated using the particle mesh Ewald method (Darden et al. 1993) with a 1.2-nm cutoff for the real-space calculation. A cutoff of 1.2 nm was also used for van der Waals interactions. The time step for integration was 2 fs, and the coordinates and velocities were saved every 40 ps for analysis. All simulations were carried out using the GROMACS package, version 4.0.7 (van der Spoel et al. 2005).

Free energy simulations

Calculating relative free energy differences has been a major subject in computational biophysics. It can help us to quantitatively understand solvation, drug binding, and protein–protein interactions at an atomistic level (Simonson et al. 2002). Commonly, free energy simulations are performed in the framework of equilibrium thermodynamics. Free energy perturbation (FEP) (Beveridge and DiCapua 1989) and thermodynamic integration (TI) (Kirkwood 1935) are two of the standard statistical mechanics methods to calculate the mutation free energies (Sun et al. 1996). The system can be represented in the calculations using either a single-topology or a dual-topology scheme (Leach 2001; Gao et al. 1989).

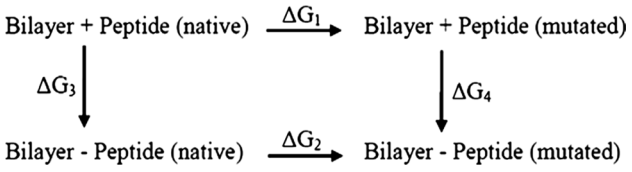

Fig. 1 Thermodynamic cycle for computing the relative binding free energies of two peptides (native and mutated) to a bilayer

To estimate the relative binding free energies of the native and mutated peptides to a bilayer, the thermodynamic cycle shown in Fig. 1 was applied. The total difference in binding affinities of these two peptides to a bilayer ($\Delta\Delta G_{\text{bind}}$) is equal to ΔG_3–ΔG_4. We notice that G is a thermodynamic state function, and this lets us consider instead

$$\Delta\Delta G_{\text{bind}} = \Delta G_3 - \Delta G_4 = \Delta G_1 - \Delta G_2 \quad (1)$$

It is computationally impractical to directly assess either ΔG_3 or ΔG_4. This means that to obtain $\Delta\Delta G_{\text{bind}}$, two simulations must be performed. The first is the transformation of native peptide to mutated peptide in a solvent environment (to calculate ΔG_1) and the other is the transformation of native peptide to mutated peptide in the bilayer environment (to calculate ΔG_2).

Free energy calculations were performed for Ile26 → Pro mutation in amylin in aqueous solution and in the bilayer, using a dual-topology description. The total size of systems in aqueous solution and in a DOPC bilayer was about 38,635 and 18,916 atoms, respectively. In this study, the coupling parameter λ was set in a range from 0.0 to 1.0 in increments of 0.05. At each λ value, the starting structure was minimized using the L-BFGS (Liu and Nocedal 1989) and steepest descents methods for up to 5,000 steps. The resulting configurations were run through an equilibration procedure consisting of 50 ps NVT equilibration, followed by 50 ps NPT equilibration. Production simulations for protein in water and in the bilayer were done for 2 and 5 ns, respectively.

Results and discussion

Structure and dynamics of the bilayer

The following macroscopic parameters of the simulated systems were analyzed using the trajectories: the density distributions of phosphorus atoms, DOPC and water

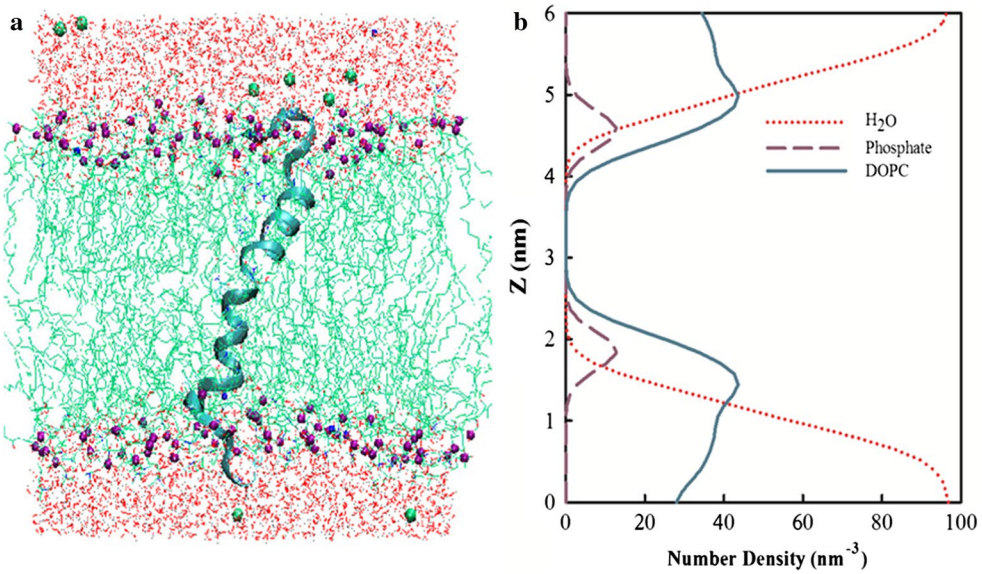

Fig. 2 **a** Simulation snapshot of the amylin in a DOPC bilayer. The peptide is shown as a *ribbon*. DOPC lipids are shown in *green*, lipid phosphate groups in *violet*, solvent molecules in *red*, Na^+ ions in *blue*, and Cl^- ions in *green*. **b** Density curves for the center of the mass for the DOPC bilayer (*blue*), phosphate groups (*violet*), and solvent molecules (*red*)

molecules along the normal to the bilayer plane, the distribution of the values of lipid order parameters over the acyl chain carbon atoms, and diffusion properties. All these parameters were averaged over MD trajectories. Analysis of the trajectories shows the behavior of the bilayer in the presence of amylin compared to available data from previous experiments and simulation studies.

The number densities, thickness, and area per lipid

A snapshot of the simulated system is shown in Fig. 2a. The number density profiles for the center of the mass of DOPC molecules, H_2O, and phosphate groups of DOPC along the axis perpendicular to the bilayer are plotted in Fig. 2b. The resulting profile is nearly symmetric, so the bilayer seems to be stable. Since the solvent molecules do not penetrate inside the hydrophobic medium, the density is zero at the center of the bilayer.

Table 1 shows the structural properties of the DOPC lipid bilayer as compared with the results from a 62-ns simulation on a DOPC lipid system with 128 lipids (with no peptide) (Bhide and Berkowitz 2005). The bilayer thickness and equilibrium average value of the area per lipid are among the most important structural parameters for lipid bilayers. These properties have been calculated by using the GridMAT-MD software (Allen et al. 2009). The bilayer thickness (measured by the phosphate-to-phosphate distance) for our simulation and from the previous results of simulation (Bhide and Berkowitz 2005) and experimental (Petrache et al. 2004 studies is 33.53, 35.08, and 36 Å, respectively. Area per lipid for the upper (64 lipid) and lower (62 lipid) leaflets of the bilayer is 68.90 and 70.39 $Å^2$. The average area per lipid for our simulation, previous simulation result, and experimental value are 69.3, 70.55, and 72.5 $Å^2$, respectively. Overall,

Table 1 Comparison of the equilibrium macroscopic averages for the DOPC bilayer in our simulations (with peptide), previous MD simulations, and experimental studies (without peptide)

Parameter average	DOPC (with peptide)	DOPC (without peptide)	
	Our simulation	Previous simulation[a]	Experiment[b]
Area per lipid ($Å^2$)	69.3 (0.10)	70.55 (0.12)	72.5
Thickness (Å)	33.53 (0.20)	35.8 (0.20)	36.9
Order parameter	0.14 (0.04)	0.10 (0.04)	0.14

The standard deviations are given in parentheses

[a] Bhide and Berkowitz (2005)

[b] The experimental value is obtained from the X-ray diffraction data and NMR spectroscopy (Petrache et al. 2004)

in comparison with the previous result (without peptide) and experimental data, there are only slight changes in the bilayer thickness, area per lipid, and order parameter. In detail, the bilayer thickness is slightly decreased because of the presence of peptide. Thus, the insertion of amylin peptide does not exert a great mechanical impact on the integrality of the whole lipid membrane.

Diffusion coefficients

The mean square displacement (MSD) contains information related to the atomic diffusivities. MSDs for DOPC lipids, head groups, and tails exhibit an increasing linear dependence with time, as shown in Figure S1 in the supporting information. DOPC lipids undergo continual structural changes in the given time interval. The slope of the MSD gives us the diffusion coefficient from the Einstein relation in two dimensions (Wohlert and Edholm 2006):

Table 2 The calculated diffusion coefficients for lipids, head groups, and tails of lipids at two dimensions for the whole time and in the last half of the simulation time

Group	Lateral diffusion ($cm^2\ s^{-1}$) 0–40 ns	Lateral diffusion ($cm^2\ s^{-1}$) 22–40 ns
DOPC	8.2×10^{-8}	7.5×10^{-8}
Head groups	6.5×10^{-8}	3.9×10^{-8}
Tails	8.9×10^{-8}	8.9×10^{-8}

$$D = \lim_{t\to\infty} \frac{\left\langle |r(t) - r(0)|^2 \right\rangle}{4t} \quad (2)$$

where $r(t)$ is the position of a particle at time t, $r(0)$ is the initial position, and < > denotes averaging over all atoms.

The MSDs for the head and tail groups and DOPC lipids change linearly in the range of 22–40 ns. The general trend observed in the lateral diffusion for a bilayer is tail > lipid > head group, as shown in Table 2 for two different time ranges. The data show that the lipid tails determine the lateral diffusion, with a negligible influence from the head groups. In mobile bilayers, the lipid chain order is an essential parameter for lipid diffusion (Wang et al. 2002; Lalchev et al. 1994). The lateral diffusion of DOPC lipids is in the order of 10^{-8} $cm^2\ s^{-1}$, depending on the time scale and on the applied force field, and is in agreement with the experimental results (Wang et al. 2002; Jacobson 1983). The values of lateral diffusion show that a DOPC bilayer possesses the property of fluidity and acts like a biological membrane.

Lipid order parameter

The lipid order parameter is a measure of the orientation mobility of the C–H bonds and is defined as follows:

$$S = \left\langle \frac{3\cos^2\theta - 1}{2} \right\rangle \quad (3)$$

where θ is the (time-dependent) angle between the C–H bond vectors and the bilayer normal (z-direction). The angular brackets denote time and ensemble averaging (Vermeer et al. 2007). The two hydrophobic tails are represented as Sn1 and Sn2 in Fig. 3b. In this work, the order parameter decreases from the interface region to the bilayer center, and the difference between the Sn1 and Sn2 chains reveals that the Sn1 tail in DOPC is more ordered in the beginning of the chain, while the Sn2 is more ordered at its end, as shown in Fig. 3a.

While there are no experimental data for direct comparison for this system, order parameters are compatible with the simulation results of fully hydrated DOPC lipid bilayers and models of β-amyloid ion channels in a DOPC lipid bilayer (Chiu et al. 1999; Jang et al. 2007). The deep dip in S_n order parameters (with n being the carbon atom sequence number in the chain) at $n = 10$ illustrates the disordering effect of the double bond. Order parameters not only depend on the (dis)order of the system, but also on the orientation (Vermeer et al. 2007). For example, an order parameter of zero in $n = 10$ shows a perfectly ordered orientation at the magic angle of 54.7°. This behavior of the double bonds is observed for both hydrophobic chains. It seems that for all biomembranes, the S parameters exhibit

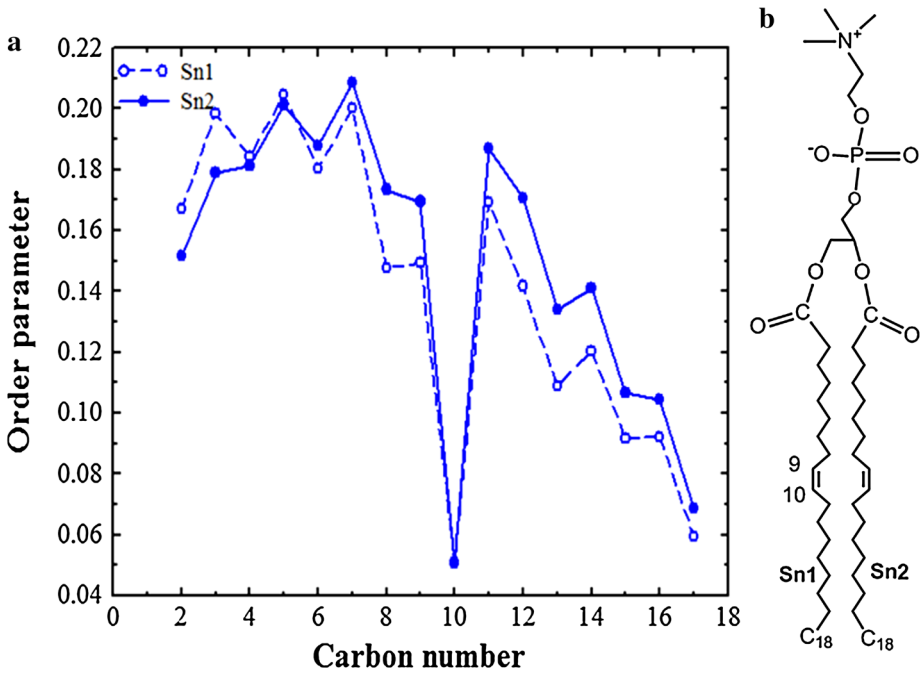

Fig. 3 **a** The order parameter as a function of the carbon number. **b** Sn1 and Sn2 hydrophobic tails. Note that the double-bonded carbon atoms are at positions 9 and 10

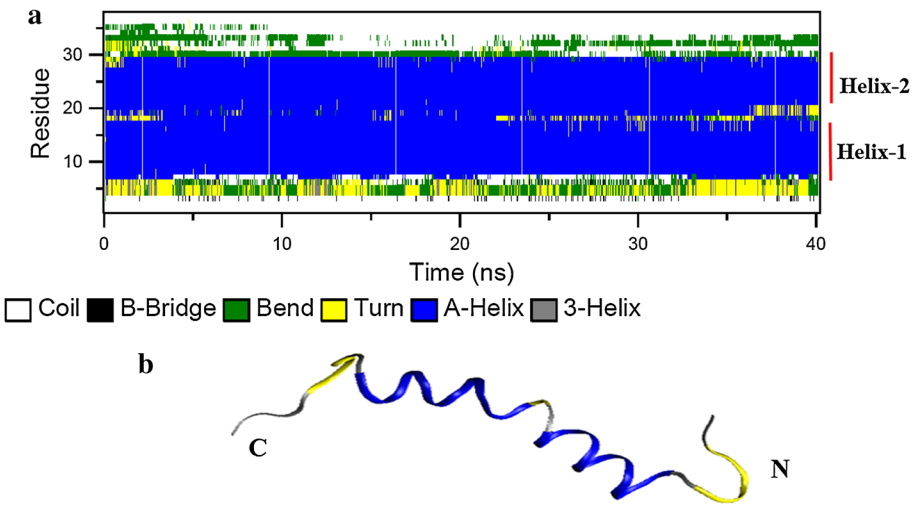

Fig. 4 **a** Time evolution of the peptide's secondary structure in 40-ns simulations. **b** A representative snapshot

a marked odd-even behavior, i.e., $S_4 < S_5$, $S_6 < S_7$, etc., especially for $T \gg T_c$ (Douliez et al. 1995). For this system, marked odd-even behavior happened until S_{11}. The average value of the order parameter for acyl chains is calculated to be 0.14 ± 0.04, which is closer to the experimental data (Petrache et al. 2004 than the result of the previous MD simulation for DOPC in the absence of peptide (Table 1).

Structure and dynamics of amylin in a DOPC bilayer

Human IAPP peptide adopts a transmembrane orientation in our study, while it lies parallel or penetrates from its N-terminal into the bilayer in other simulations (Jia et al. 2013; Williamson et al. 2009). After 40 ns simulation time, the peptide molecule maintains its structure and does not exit from the bilayer, so it does not have a toxic effect on the bilayer.

Secondary structure

Analysis of the secondary structures in amylin peptide has been performed using the DSSP program (Kabsch and Sander 1983). The secondary structure of the peptide is depicted as a function of time in Fig. 4. As is clear from this plot and the representative snapshot in Fig. 4, a distortion or kink near residues 18–22 introduces pliancy in the angle between the N- and C-terminal segments of the α-helix. The kink region is between Ser19 and Asn22. The first four residues in the structure are constrained to form a hairpin loop by the single disulfide bond in amylin. The last nine residues near the C-terminal are structureless. During the time of 13–25 ns they are coiled, and at other times they are almost bent. These results agree well with the analysis of a set of structures of the peptide bound to sodium dodecyl sulfate (SDS) micelles obtained by NMR spectroscopy at pH = 7 (Patil et al. 2009).

Peptide dynamics

The time evolution of the root mean square displacement (RMSD) from the initial structure is plotted for the center of mass of amylin in a DOPC bilayer in Fig. 5. The main conformational changes occur during the first 22 ns of the simulation. At this stage, RMSD from the starting structure arrives at its maximum value (0.65 nm) and then remains unchanged. The trends in RMSD indicate that this structure is stable. The behavior of protein and its backbone is similar, but because of the higher flexibility of sidechain atoms, the RMSD for protein is higher than the backbone RMSD at each time.

Since the distance deviations from the starting structure may not necessarily reflect the mobility of the structural elements, relative flexibilities of protein residues were estimated based on the values of their root mean square fluctuation (RMSF), averaged over 40 ns. The RMSF is the root mean square deviation with respect to the mean structure that can be obtained for each particle by averaging over time. The RMSD per residue is similar to RMSF; however, the reference is some special structure (e.g., initial structure) rather than the mean structure. The RMSFs per residue for the center of mass of the peptide and backbone as well as the RMSD per residue for the center of mass of the peptide are displayed in Fig. 6. It is clear that both the C- and N-termini have large motions, but the C-terminus is more flexible. Moreover, the mobilities of Cys7, Ala8, Leu12, and Leu16 are significant. Because each residue is more flexible than the backbone of that residue, RMSF values for peptide are more than those for backbone RMSFs. It is interesting that RMSDs are more than RMSFs for each residue.

Free energy analysis

The free energy difference between the native and mutated states of the amylin peptide is given by

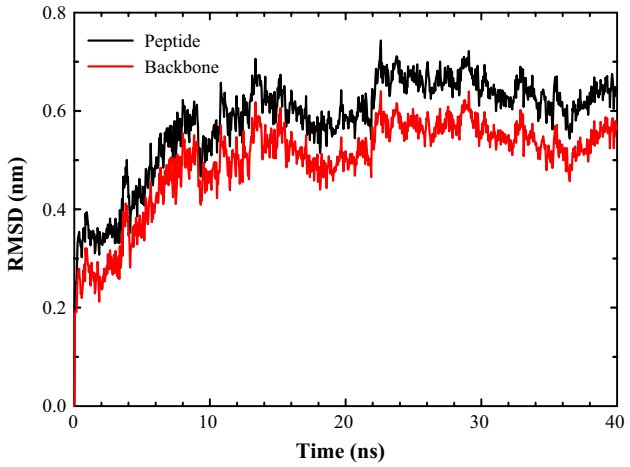

Fig. 5 Time evolution of RMSD measured from the corresponding starting structure. RMSDs of peptide and backbone atoms are shown by *black* and *red lines*, respectively

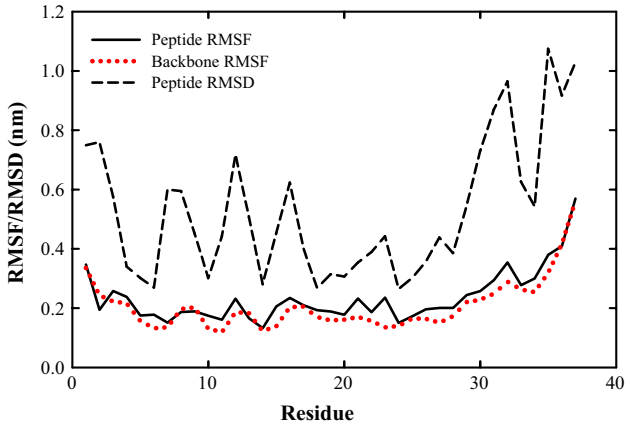

Fig. 6 RMSF and RMSD per residue for amylin peptide averaged over 40 ns

$$\Delta G = \int_0^1 \left\langle \frac{dH(\lambda)}{d\lambda} \right\rangle_\lambda d\lambda \tag{4}$$

It is assumed that G is a continuous function of the coupling parameter, λ. The $< >_\lambda$ represents an ensemble average. This integral is numerically evaluated over a number of equilibrated intermediate values of λ, or windows. Since the kinetic energy contribution can be neglected in a stability study (van Gunsteren et al. 1989; Kollman 1993), in practice, Eq. (5) can be approximated using the trapezoidal rule to calculate the free energy change:

$$\Delta G \cong \sum_i \left\langle \frac{dV(\lambda)}{d\lambda} \right\rangle_{\lambda_i} \Delta\lambda \tag{5}$$

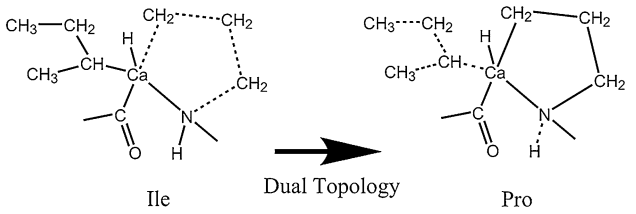

Fig. 7 The mutation of the Ile26 → Pro in a dual topology representation. The *dashed part* of the cartoons represents the part of the total Hamiltonian that is 'zeroed' in the Hamiltonian H (λ)

where λ_i refers to the λ value at the ith window (van Gunsteren et al. 1989; Kollman 1993).

The dual-topology approach has been used in this study, as illustrated in Fig. 7. The dashed part of the cartoons shows the part of the total Hamiltonian, which is zeroed in the mutation Hamiltonian H(λ). The noncovalent force parameters of the atoms on the dashed part of the cartoons are all set to zero. The dashed lines represent that the covalent force constants associated with these atoms are also mutated to zero as well at the end points λ = 0 and 1.0. To ensure having well-equilibrated systems, free energy gradients dG/dλ versus time are plotted for λ = 0.0, 0.5, and 1.0 for simulations in both the bilayer and aqueous environment (Fig. 8). It is clear that the dG/dλ, although fluctuating, remains fairly constant over the entire simulation.

It can be observed in Fig. 9 that <dG/dλ> versus λ increases monotonously from λ = 0 to 1 for amylin in a bilayer, whereas it shows a sudden increase from λ = 0.7 in solvent, which corresponds to the unfolding of the peptide at these states in a solvent environment. Also, in Fig. 10, it is shown that the amount of α-helix in the mutated peptide reduces to 5-helix in aqueous solution, whereas this configuration is preserved in the bilayer. It seems that a native amylin loses its structure in aqueous solution, as depicted in Figure S2.

About 20 simulations were done for each mutation in both the free state to get ΔG_1 (I26P in an aqueous solution) and in the bound state to yield ΔG_2 (I26P in a DOPC bilayer). From these simulations, we have

$$\Delta\Delta G_{\text{bind}} = \Delta G_1 - \Delta G_2 = 28.71 - 2.69 = 26.02\ \text{kJ.mol}^{-1} \tag{6}$$

These findings suggest that the process of mutation for peptide in a membrane environment ($\Delta G_2 = 2.69$) is more favorable than in a solvent environment ($\Delta G_1 = 28.71$). Since the $\Delta\Delta G_{\text{bind}}$ value is positive, it can be deduced that the native peptide binds to a DOPC bilayer better than the mutated peptide. The mutated peptide loses some of the hydrogen bonds upon the disruption of the helical structure, so it tends to bind to the bilayer.

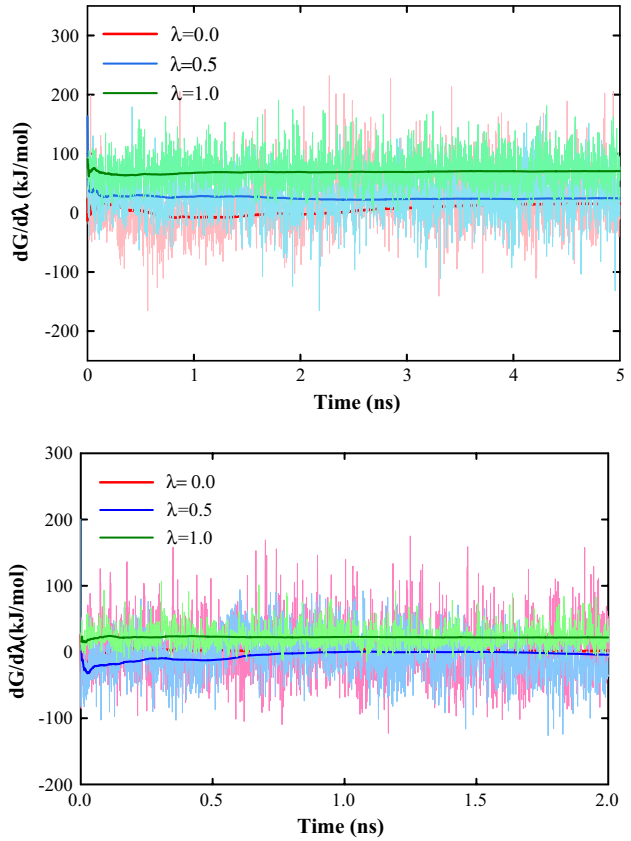

Fig. 8 Free energy gradients (dG/dλ) versus time for the mutation of peptide in both the bilayer (*top*) and aqueous solution (*bottom*). The cumulative averages are shown using *red*, *blue*, and *green solid lines* for λ = 0.0, 0.5, and 1.0, respectively

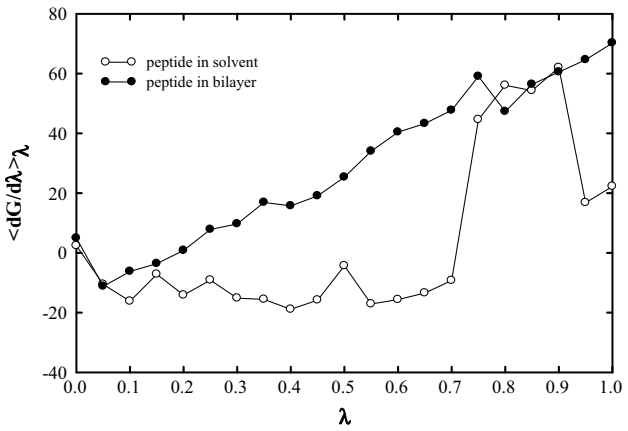

Fig. 9 Free energy derivations for the mutation of peptide in both aqueous and bilayer environments with respect to λ (in kJ.mol^{-1})

Since the hydrophobic interaction is one of the most important driving forces of protein aggregations (Baumketner and Shea 2007), we have calculated the solvent-accessible surface areas (SASAs) per residue for hIAPP to evaluate the contribution of the hydrophobic interaction to the assembly of peptide. The solvent-accessible surface area reflects the percentage of the surface area of a given residue that is accessible to the solvent. It can be related to the hydrophobic core and is typically calculated using the 'rolling ball' algorithm (Shrake and Rupley 1997; Doss and NagaSundaram 2012).

Upon mutation, the SASA for peptide in a solvent environment is increased, as displayed in Table 3. An accessible area quota change for hydrophilic residues in a solvent environment is more than these changes in a membrane environment during the mutation. It can be deduced that intermolecular hydrogen bonds are broken and new hydrogen bonds form between the peptide and surrounding solvents. The accessible area for hydrophobic residues is greater than that for hydrophilic residues for each environment and each λ. A decrease or increase in the solvent-accessible surface area indicates the change in exposed residues, and it could affect the tertiary structure of the peptide. The numbers of hydrogen bonds formed between native hIAPP and the lipid bilayer in λ = 0 and between mutated hIAPP and the lipid bilayer in λ = 1 are shown in figure S4. The number of hydrogen bonds formed in native hIAPP is more than the number of hydrogen bonds formed between native hIAPP and the lipid bilayer, whereas the number of hydrogen bonds formed between mutated hIAPP and the lipid bilayer is more than in mutated hIAPP.

Conclusions

MD simulations of native amylin peptide in a dioleoylphosphatidylcholine (DOPC) bilayer were performed at 323 K for 40 ns. Structural properties such as the RMSD, RMSF, and the secondary structure of peptide were evaluated from these trajectories. The secondary structure of amylin peptide shows that the amino acids in two termini are structureless and two α-helix segments in the peptide are connected through an unstructured link. The results of classical MD simulations presented here are consistent with the experimental observations and simulations.

The effect of I26P mutation on binding of amylin peptide to a DOPC bilayer is not available from experimental data. In order to find this, free energy changes for the transformation of the native peptide to mutated peptide in both solvent and the bilayer environments were computed. The computed relative free energy of binding $\Delta\Delta G_{\text{bind}}$ is 26.05 kJ mol^{-1}. These findings suggest that the process of mutation for peptide in a solvent environment is more desirable than in a membrane environment. Upon mutation, the accessible surface area for hydrophobic residues is greater than that

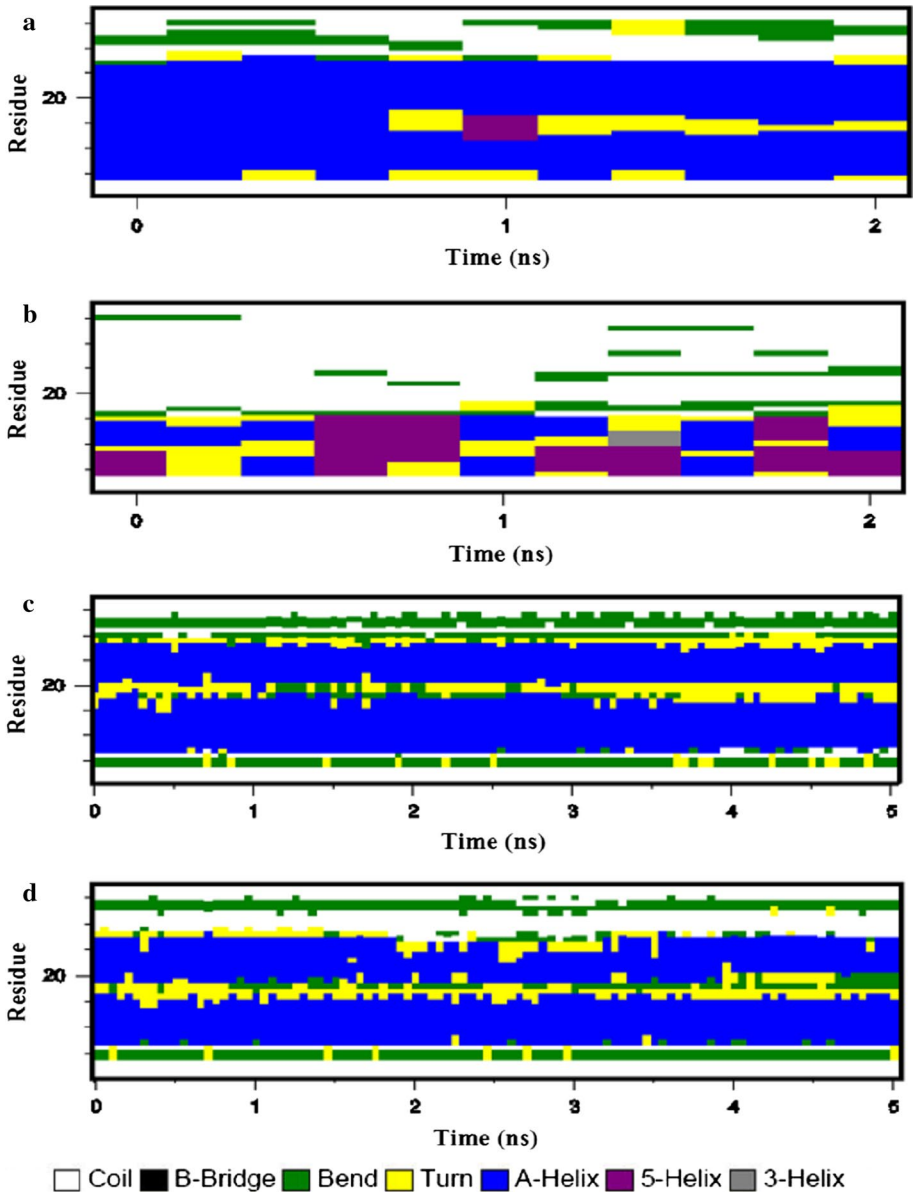

Fig. 10 Time evolution of the peptide's secondary structure for (**a**) amylin in water solvent at $\lambda = 0$ (**b**) and amylin in water solvent at $\lambda = 1$. (**c**) Amylin in a DOPC bilayer at $\lambda = 0$ (**d**). Amylin in a DOPC bilayer at $\lambda = 1$

Table 3 Solvent accessible surface area for hydrophobic and hydrophilic residues for $\lambda = 0$ and $\lambda = 1$ in both solvent and bilayer environments

SASA (nm^2)	$\lambda = 0$			$\lambda = 1$		
	Hydrophobic	Hydrophilic	Total	Hydrophobic	Hydrophilic	Total
Peptide in solvent	22.7358	17.4472	40.1830	22.3094	20.5447	42.9279
Peptide in bilayer	11.4683	7.7224	19.1907	10.8664	7.4642	18.3306

for hydrophilic residues for each environment and each λ. It is interesting that accessible surface areas increase for hydrophobic residues in the bilayer environment and for hydrophilic residues in aqueous solution when the mutation happens. This detailed information about the peptide in a bilayer and relative free energy for the binding of native and mutated peptide to a bilayer gives insight into the structure and mechanism of protein stability in detail.

Acknowledgments This work was supported by the Theoretical and Computational Physical Chemistry Laboratory at K.N. Toosi University of Technology.

References

Abedini A, Meng F, Raleigh DP (2007) A single-point mutation converts the highly amyloidogenic human islet amyloid polypeptide into a potent fibrillization inhibitor. J Am Chem Soc 129:11300–11301

Allen WJ, Lemkul JA, Bevan DR (2009) Gridmatmd: a grid-based membrane analysis tool for use with molecular dynamics. J Comput Chem 30:1952–1958

Baumketner A, Shea J (2007) The structure of the Alzheimer amyloid ß 10–35 peptide probed through replica-exchange molecular dynamics simulations in explicit solvent. J Mol Biol 366:275–285

Berendsen HJC, Postma JPM, van Gunsteren WF, Hermans J (1981) Interaction models for water in relation to protein hydration. In: Pullman B (ed) Intermolecular forces. D. Reidel Publishing Company, Dordrecht, pp 331–342

Berger O, Edholm O, Jhnig F (1997) Molecular dynamics simulations of a fluid bilayer of dipalmitoylphosphatidylcholine at full hydration, constant pressure, and constant temperature. Biophys J 72:2002

Betsholtz C, Christmansson L, Engstrom U, Rorsman F, Svensson V, Johnson KH, Westermark P (1989) Sequence divergence in a specific region of islet amyloid polypeptide (IAPP) explains differences in islet amyloid formation between species. FEBS Lett 251:261–264

Beveridge DL, DiCapua FM (1989) Free energy via molecular simulation: applications to chemical and biomolecular systems. Ann Rev Biophys Biophys Chem 18:431–492

Bhide SY, Berkowitz ML (2005) Structure and dynamics of water at the interface with phospholipid bilayers. J Chem Phys 123:224702

Chiu SW, Jakobsson E, Subramaniam S, Scott HL (1999) Combined monte carlo and molecular dynamics simulation of fully hydrated dioleyl and palmitoyl-oleyl phosphatidylcholine lipid bilayers. Biophys J 77:2462–2469

Darden T, York D, Pedersen L (1993) Particle mesh Ewald: an N.log (N) method for Ewald sums in large systems. J Chem Phys 98:10089–10092

Doss CGP, NagaSundaram N (2012) Investigating the Structural Impacts of I64T and P311S Mutations in APE1-DNA complex: a molecular dynamics approach. PLoS One 7:e31677

Douliez J-P, Leonard A, Dufourc EJ (1995) Restatement of order parameters in biomembranes: calculation of C–C bond order parameters from C–D quadrupolar splitting. Biophys J 68:1727–1739

Duan M, Fan J, Huo S (2012) Conformations of islet amyloid polypeptide monomers in a membrane environment: implications for fibril formation. PLoS One 7:e47150

Dupuis NF, Wu C, Shea JE, Bowers MT (2011a) The amyloid formation mechanism in human IAPP: dimers have beta-strand monomer-monomer interfaces. J Am Chem Soc 133:7240–7243

Dupuis NF, Wu C, Shea J, Bowers MT (2011b) J Am Chem Soc 133:7240

Engel MFM, Yigittop H, Elgersma RC, Rijkers DTS, Liskamp RMJ, de Kruijff D, HÖppener JWM, Killian JA (2006) Islet amyloid polypeptide inserts into phospholipid monolayers as monomer. J Mol Biol 356:783–789

Fowler PW, Jha S, Coveney PV, Wan S (2004) Exact calculation of peptide-protein binding energies by steered thermodynamic integration using high performance computing grids. In: proceedings of the UK e-Science All Hands Meeting

Gao J, Kuczera K, Karplus M (1989) Hidden thermodynamics of mutant proteins: a molecular dynamics analysis. Science 244:1069–1072

Garcia-Gonzalez CL, Montoya-Fuentes H, Padilla-Rosas M, Sanchez-Corona G (2007) Amylin S20G mutation in Mexican population. Diabetes Res Clin Pract 76:146–148

Hess B, Bekker H, Berendsen HJC, Feraaije JGEM (1997) LINCS: a linear Constrain solvent for molecular simulations. J Comput Chem 18:1463–1472

Jacobson K (1983) Lateral diffusion in membranes. Cell Motil 3:367–373

Jaikaran ETAS, Clark A (2001) Islet amyloid and type 2 diabetes: from molecular misfolding to islet pathophysiology. Biochim Biophys Acta 1537:179–203

Jaikaran E, Higham CE, Serpell LC, Zurdo J, Gross M, Clark A, Fraser PE (2001) Identification of a novel human islet amyloid polypeptide beta-sheet domain and factors influencing fibrillogenesis. J Mol Biol 308:515–525

Jang H, Zheng J, Nussinov R (2007) Models of β-Amyloid ion channels in the membrane suggest That channel formation in the bilayer is a dynamic process hyunbum. Biophys J 93:1938–1949

Jia Y, Qian Z, Zhang Y, Wei G (2013) Adsorption and orientation of human islet amyloid polypeptide (hIAPP) monomer at anionic lipid bilayers: implications for membrane-mediated aggregation. Int J Mol Sci 14:6241–6258

Jiang P, Xu W, Mu Y (2009) Amyloidogenesis abolished by proline substitutions but enhanced by lipid binding. PLoS Comput Biol 5:e1000357

Kabsch W, Sander C (1983) Dictionary of protein secondary structure: pattern-recognition of hydrogen-bonded and geometrical features. Biopolymers 22:2577–2637

Kandt C, Ash WL, Tieleman DP (2007) Setting up and running molecular dynamics simulations of membrane proteins. Methods 41:475–488

Karlsson E (1999) IAPP as a regulator of glucose homeostasis and pancreatic hormone secretion (review). Int J Mol Med 3:577–584

Khemtemourian L, Killian JA, Hoppener JW, Engel MFM (2008) Recent insights in islet amyloid polypeptide-induced membrane disruption and its role in β-cell death in type 2 diabetes mellitus. Experimental Diabetes Research 2008:421287

Kirkwood JG (1935) Statistical mechanics of fluid mixtures. J Chem Phys 3:300–313

Kollman PA (1993) Free energy calculations: applications to chemical and biochemical phenomena. Chem Rev 93:2395–2417

Laghaei R, Mousseau N, Wei GH (2011) Structure and thermodynamics of amylin dimer studied by hamiltonian-temperature replica exchange molecular dynamics simulations. J Phys Chem B 115:3146–3154

Lalchev ZI, Wilde PJ, Clark DC (1994) Surface diffusion in phospholipids foam films. Colloids Surf 167:80

Leach AR (2001) Molecular modeling. Principles and applications, 2nd edn. Pearson Education Limited, UK

Liu D, Nocedal J (1989) On the limited memory method for large scale optimization. Math Program Ser B 45:503–528

Lopes DHJ, Meister A, Gohlke A, Hauser A, Blume A, Winter R (2007) Mechanism of islet amyloid polypeptide fibrillation at lipid interfaces studied by infrared reflection absorption spectroscopy. Biophys J 93:3132–3141

Mo Y, Lu Y, Wei G, Derreumaux P (2009) Structural diversity of the soluble trimers of the human amylin (20–29) peptide revealed by molecular dynamics simulations. J Chem Phys 130:125101–125106

Oostenbrink C, Villa A, Mark AE, Gunsteren WFV (2004) A biomolecular force field based on the free enthalpy of hydration and solvation: the GROMOS force field parameter sets 53A5 and 53A6. J Comput Chem 25:1656–1676

Patil SM, Xu S, Sheftic SR, Alexandrescu AT (2009) Dynamic α-Helix structure of micelle-bound human amylin. J Biol Chem 284:11982–11991

Petrache HI, Tristram-Nagle S, Gawrisch K, Harries D, Parsegian VA, Nagle JF (2004) Structure and fluctuations of charged phosphatidylserine bilayers in the absence of salt. Biophys J 86:1574–1586

Sakagashira S, Hiddinga HJ, Tateishi K, Sanke T, Hanabusa T, Nanjo K, Eberhardt NL (2000) S20G mutant amylin exhibits increased in vitro amyloidogenicity and increased intracellular cytotoxicity compared to wildtype amylin. Am J Pathol 157:2101–2109

Sciacca MFM, Pappalardo M, Attanasio F, Milardi D, La Rosa CM, Grasso D (2010) Are fibril growth and membrane damage linked processes? An experimental and computational study of IAPP (12–18) and IAPP (21–27) peptides. New J Chem 34:200–207

Shrake A, Rupley JA (1997) Environment and exposure to solvent of protein atoms lysozyme and insulin. J Mol Biol 79:351–371

Simonson T, Archontis G, Karplus M (2002) Free-energy simulations come of age: protein-ligand recognition. Acc Chem Res 35:430–437

Sun Y-C, Veenstra DL, Kollman PA (1996) Free energy calculations of the mutation of De96 → Ala in barnase: contributions to the difference in stability. Protein Eng 9:273–281

Tristram-Nagle S, Petrache HI, Nagle JF (1998) Structure and interactions of fully hydrated dioleoylphosphatidylcholine bilayers. Biophys J 75:917

van der Spoel D, Lindahl E, Hess B, Groenhof G, Mark AE, Berendsen HJC (2005) GROMACS: fast, flexible and free. J Comput Chem 26:1701–1718

van Gunsteren WF, Weiner P, Editors (1989) Computer simulation of biomolecular systems: Theoretical and experimental applications, ESCOM 1 Leiden, The Netherlands

Vermeer LS, de Groot BL, Reat V, Milon A, Czaplicki J (2007) Acyl chain order parameter profiles in phospholipid bilayers: computation from molecular dynamics simulations and comparison with ^{2}H NMR experiments. Eur Biophys J 36:919–931

Wang L, Schonhoff M, Mohwald H (2002) Lipids coupled to polyelectrolyte multilayers: ultraslow diffusion and the dynamics of electrostatic interactions. J Phys Chem B 106:9135–9142

Wang M, Yang J, Wang J, Wang X (2012) Structural Effects of L16Q, S20G, and L16Q-S20G Mutations on hIAPP: a comparative molecular dynamics study. Chin J Chem 30:241–248

Westermark P (1973) Fine structure of islets of Langerhans in insular amyloidosis. Virchows Archiv A 359:1–18

Westermark P, Wernstedt C, Wilander E, Hayden DW, O'Brien TD, Johnson KH (1987) Amyloid fibrils in human insulinoma and islets of Langerhans of the diabetic cat are derived from a neuropeptide-like protein also present in normal islet cells. Proc Natl Acad Sci USA 84:3881–3885

Williamson JA, Loria JP, Miranker AD (2009) Helix stabilization precedes aqueous and bilayer-catalyzed fiber formation in islet amyloid polypeptide. J Mol Biol 393:383–396

Wohlert J, Edholm O (2006) Dynamics in atomistic simulations of phospholipid membranes: nuclear magnetic resonance relaxation rates and lateral diffusion. J Chem Phys 125:204703

Xu W, Ping J, Li W, Mu Y (2009) Assembly dynamics of two-beta sheets revealed by molecular dynamics simulations. J Chem Phys 130:164709. http://www.bioinf.uni-sb.de/RB/dopc/berger/berger-NPT-100ns.pdb

Zhang Y, Luo Y, Deng Y, Mu Y, Wei G (2012) Lipid interaction and membrane perturbation of human islet amyloid polypeptide monomer and dimer by molecular dynamics simulations. PLoS One 7(5):e38191